Molecular Dynamics Simulations of Solvated Yeast tRNA^{Asp}

Pascal Auffinger, Shirley Louise-May, and Eric Westhof

Institut de Biologie Moléculaire et Cellulaire du CNRS, Modélisations et Simulations des Acides Nucléiques, UPR 9002, 67084 Strasbourg Cedex, France

ABSTRACT   Transfer RNA molecules are involved in a variety of biological processes, implying complex recognition events with proteins and other RNAs. From a structural point of view, tRNAs constitute a reference system for studying RNA folding and architecture. A deeper understanding of their structural and functional properties will derive from our ability to model accurately their dynamical behavior. We present the first dynamical model of a fully neutralized and solvated tRNA molecule over a 500-ps time scale. Starting from the crystallographic structure of yeast tRNA^{Asp}, the 75-nucleotide molecule was modeled with 8055 water molecules and 74 NH$_4^+$ counterions, using the AMBER4.1 program and the particle mesh Ewald (PME) method for the treatment of long-range electrostatic interactions. The calculations led to a dynamically stable model of the tRNA molecule. During the simulation, all secondary and tertiary base pairs are maintained while a certain lability of base triples in the tRNA core is observed. This lability was interpreted as resulting from intrinsic factors associated with the "weaker" hydrogen bonding patterns seen in these base triples and from an altered ionic environment of the tRNA molecule. Calculated thermal factors are used to compare the dynamics of the tRNA in solution and in the crystal. The present molecular dynamics simulation of a complex and highly charged nucleic acid molecule attests to the fact that simulation methods are now able to investigate not only the dynamics of proteins, but also that of large RNA molecules. Thus they also provide a basis for further investigations on the structural and functional effects of chemical and posttranscriptionally modified nucleotides as well as on ionic environmental effects.

INTRODUCTION

Transfer RNAs belong to the first class of functional nucleic acid molecules for which three-dimensional structures were determined by x-ray crystallography (for a review, see Dirheimer et al., 1995). To help unravel their structural determinants and unique specificities, the structural interactions of base pairs, base triples, modified bases, hairpins, and coaxially stacked helices have been studied by sequence mutation, chemical, and solution probing, as well as theoretical modeling (see Söll and RajBhandary, 1995). Key interaction sites, concentrated in the two ends and the "elbow" of the L-shaped structure, include the 3′-CCA residues of the acceptor stem involved in aminoacylation, the anticodon residues, which interact with the cognate synthetase and the cognate-related codon of the mRNA, as well as the TΨC loop, which contains the most conserved sequence of modified residues in tRNA and acts as a recognition element for elongation factors and ribosomal RNA sites.

Fifteen years ago, McCammon and Harvey undertook the first large-scale molecular dynamics (MD) studies of an RNA molecule: the 76-nucleotide yeast tRNA^{Phe} (for a review, see McCammon and Harvey, 1987). These calculations were extremely challenging at the time, when the largest DNA simulations comprised only 24 nucleotides. In their model, solvation was implicit and the effect of the counterions was approximated by reducing the atomic charges on the phosphate groups. Although the hydrogen bonds of the secondary structure were maintained during the 32-ps MD trajectory, several important tertiary interactions broke, reflecting severe methodological difficulties and impeding the extension of the MD trajectory toward longer time scales. Subsequent MD studies demonstrated that methodological problems, due to shortcomings in the treatment of electrostatic interactions, are revealed by a rapid alteration of the tertiary structure and unphysical dynamical behavior of charged residues (Ravishanker et al., 1997; Tapia and Velazquez, 1997). Among nucleic acids, these problems became most noticeable for RNA molecules that display complex tertiary folds of their highly charged polynucleotidic chain (Westhof et al., 1995). Improved methods for the treatment of electrostatic forces such as the particle mesh Ewald (PME) methods, which were recently introduced in MD simulations of biomolecules (Darden et al., 1993; Essmann et al., 1995), have demonstrated the absolute necessity of taking explicitly into account the often neglected long-range part (beyond 8–10 Å) of the electrostatic interactions. These methods allow one to generate stable MD trajectories extending into the nanosecond range for completely solvated and neutralized nucleic acid systems (see Auffinger and Westhof, 1998c).

Previous work on fragments of yeast tRNA^{Asp} using a variety of MD protocols has led to the identification of some important structural features previously not considered. The anticodon loop structure was found to be stabilized, in addition to the well-characterized base-phosphate interaction at the U-turn level, by a single bifurcated hydrogen bond linking residues 32 and 38 and by two C-H⋯O inter-
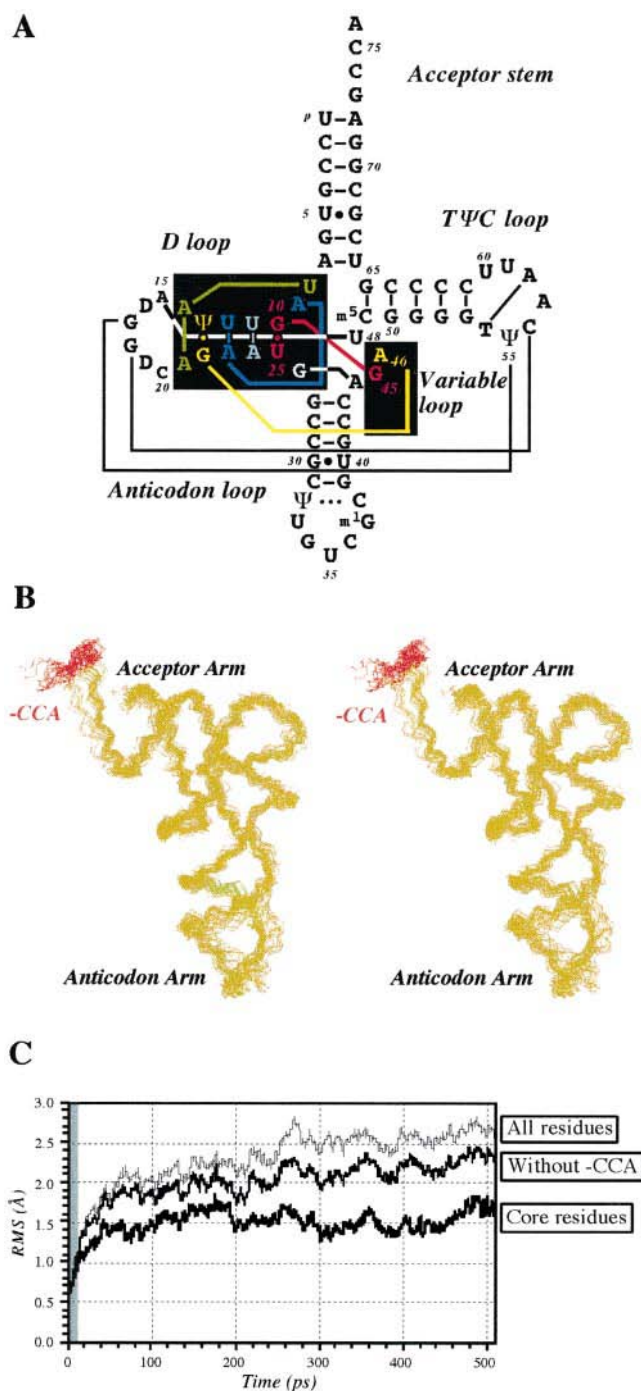
FIGURE 1 (*A*) Yeast tRNA^{Asp} secondary structure, including the pseudouridine (Ψ), dihydrouridine (D), 1-methylguanine (m^{1}G), 5-methylcytosine (m^{5}C), and ribothymine (T) modified residues. The numbering is not continuous, so as to conform to the numbering of yeast tRNA^{Phe} (Quigley and Rich, 1976). The numbering around the two invariant G residues of the D loop is -D16-G17-G18-D19-C20- in tRNA^{Asp} and -D16-D17-G18-G19-G20- in tRNA^{Phe} (Westhof et al., 1985). Tertiary base-base interactions are indicated by solid lines. The color code is the same as the one used in Fig. 7. (*B*) Stereo view of the superposition of the backbone of 25 structures extracted at 20-ps intervals from the 500-ps MD trajectory (the backbone of the tRNA is in *green ochre*; the backbone of the terminal -CCA residues is in *red*). (*C*) Time course of the RMS deviations from the starting structure (the 10 ps of equilibration is shaded in gray; see Computational Procedure). The thin top line corresponds to the RMS deviations calculated for the entire tRNA, the middle line has been obtained by

actions involving the conserved U33 residue (Auffinger et al., 1996b; Auffinger and Westhof, 1996). The importance of long-lived (in the nanosecond range) hydration patterns in the stabilization of the loop structure was demonstrated (Auffinger and Westhof, 1997a), and modified nucleotides were found to contribute to the stabilization of these long-lived hydration patterns (Auffinger and Westhof, 1997a; 1998a). Furthermore, stereochemical rules specifying the allowed orientations of the RNA 2′-hydroxyl ribose groups and their role in protein/RNA or RNA/RNA interactions were derived from MD simulations (Auffinger and Westhof, 1997b). To enhance the statistical significance of results derived from these calculations, the multiple molecular dynamics (MMD) strategy was used. This strategy, which consists of generating an ensemble of uncorrelated trajectories by perturbing slightly the initial conditions of the simulations, exploits the chaotic stochastic nature of MD runs (Auffinger and Westhof, 1998b). Recently, MD simulations were conducted on the 41-nucleotide-long hammerhead ribozyme, leading to a new proposal for its reaction mechanism (Hermann et al., 1997; 1998). Yet indeed, because of their size, the MMD strategy could not be applied to a molecule of the size of the hammerhead ribozyme or tRNA molecule molecules.

The present 500-ps MD investigation, undertaken on the whole yeast tRNA^{Asp} molecule (75 nucleotides; Fig. 1), surrounded by 8055 explicit water molecules and 74 NH$_4^+$ counterions, was carried out to test current MD protocols on a larger and more challenging system. It is worth noting that the model of yeast tRNA^{Asp} does not include Mg^{2+} ions, as none had been detected by crystallography, presumably because of the use of a highly concentrated ammonium sulfate crystallization buffer (Westhof et al., 1985). Thus to reproduce the ionic environment in the crystal, NH$_4^+$ counterions were placed around the tRNA molecule.

From the biochemical point of view, simulations of a tRNA molecule provide the opportunity to investigate the stability of tertiary base pairs and base triples, which are mainly present in the core of the tRNA molecule. Most of these tertiary interactions involve bases that are invariant or semiinvariant and thus are structurally important. Furthermore, the study of the stability of base triples is of importance because they are involved in the stabilization of complex tertiary folds not only in tRNAs but also in large ribozymes such as the group I intron (Michel and Westhof, 1990) and RNA aptamers (Patel et al., 1997). Furthermore, the aim of this study was to investigate the dynamics of the different regions constituting the L-shaped tRNA molecule such as the anticodon hairpin, the acceptor arm extremities, and the core of the tRNA, where all of the base triples cluster.

excluding from the RMS calculation the three pending and highly mobile -CCA nucleotides at the 3′ end of the acceptor stem, and the bold bottom line has been obtained by calculating the RMS deviations for the residues with experimental B-factors lower than 15 Å^2 (residues 6–15, 22–31, 39–53, and 61–67). These residues constitute the core of the tRNA molecule (see Fig. 1 *A*).

From a methodological point of view, the results of the simulation are first analyzed with respect to global RMS deviations to evaluate the quality of the trajectory. Then, with the aim of determining the importance of crystal packing effects on the mobility of the tRNA molecule, calculated and experimental temperature factors are compared. Finally, the fine structure of the tRNA at the hydrogen bonding level is analyzed.

COMPUTATIONAL PROCEDURES

The starting coordinates were extracted from the tRNA^{Asp} A-form crystal structure (Westhof et al., 1988) (NDB code tRNA07; Berman et al., 1992). In this structure, a Watson-Crick interaction links base G18 of the D loop to base C56 of the TΨC loop (Fig. 1 *A*). The 75-nucleotide tRNA molecule was surrounded by 74 NH_4^+ counterions and 8055 SPC/E water molecules (Berendsen et al., 1987) filling a $103.2 \times 33.7 \times 32.7$ Å^3 rectilinear box. The counterions were placed based on the electrostatic potential of the solvated system such that no counterion was closer than 4.5 Å to any solute atom or closer than 3.5 Å to any other counterion. For the treatment of the long-range electrostatic interactions, the particle mesh Ewald (PME) method (Darden et al., 1993; Essmann et al., 1995), as implemented in the AMBER4.1 package (Pearlman et al., 1994), was used. A 9.0-Å truncation distance was applied to the Lennard-Jones interactions. The charge grid spacing was chosen to be close to 1.0 Å, and a cubic interpolation scheme was used. The trajectory was run at a constant temperature of 298 K and a constant pressure of 1 atm, with a time step of 2 fs. The nonbonded pair list was updated every 10 steps. As in our previous investigations on the dynamics of RNA fragments (Auffinger et al., 1996a,b; Auffinger and Westhof, 1996), the Pearlman and Kim (1990) set of electrostatic charges, derived from low-temperature x-ray studies on isolated nucleotides, was used.

An equilibration protocol similar to those used in our preceding work (Auffinger et al., 1996a,b; Auffinger and Westhof, 1996) was applied. This equilibration protocol consisted of 100 steps of steepest descent minimization, followed by 5 ps of MD at 298 K applied to the water molecules to relax the initial strain present at the RNA/solvent interface. Next, the water molecules and NH_4^+ counterions were allowed to relax at 100 K (1 ps), 200 K (1 ps), and 300 K (5 ps) around the fixed RNA molecule. In succeeding steps, no positional constraints were applied to the system, and the temperature was progressively increased to 298 K in steps of 50 K with 1 ps of MD at each step. Finally, at 298 K, 5 ps of dynamics was run to allow the system to relax at room temperature, concluding the equilibration and thermalization process, which lasted 22 ps. The production phase consisted of 500 ps of unrestrained molecular dynamics on the fully solvated and neutralized tRNA system. The MDdraw program (Engler and Wipff, 1994) was used to visualize the generated trajectory on a

Silicon Graphics workstation. The calculation took ~3 weeks of CPU time on a CRAY YMP machine.

RESULTS

Global RMS deviations

To get a rough estimate of the quality of the MD trajectory, the all-atom root mean square (RMS) deviations from the starting crystal structure were calculated (Fig. 1 *C*). After a rapid increase during the first 100 ps, the all-atom RMS deviations drifted slowly from an average of 2.2 Å to 2.7 Å between 100 and 500 ps. These low RMS deviations are in the range of those calculated from MD simulations of smaller nucleic acid systems by other groups using Ewald summation methods (Cheatham et al., 1995; Weerasinghe et al., 1995a,b; Yang and Pettitt, 1996; Young et al., 1997; Hermann et al., 1998) and indicate that the trajectory remained globally close to the reference crystallographic structure. However, the large final difference (0.4 Å) between the RMS deviations calculated with and without the inclusion of the pending 3′-CCA nucleotides of the acceptor stem point (Fig. 1 *C*), in agreement with their high crystallographic thermal factors, points to the large mobility of these residues in solution (Westhof et al., 1988). The RMS deviations for the core residues (core residues are defined as those displaying B-factors below 15 Å^2 in the crystal) fluctuate around 1.5 Å and do not drift toward higher values after the first 200 ps of simulation. This last result reveals a good overall preservation of the constrained structure of the core of the tRNA and indicates that the motions of the acceptor and anticodon extremities account mainly for the drifts observed in the all-atom RMS profiles. Such behavior is anticipated for nonglobular systems like tRNA molecules.

To sample more completely the conformational space of large macromolecules, multiple molecular dynamics runs (Auffinger and Westhof, 1998b) associated with longer simulation times may be required (Caspar, 1995; Clarage et al., 1995). However, the present apparently short 500-ps time scale is sufficient to gain novel insights into the intrinsic dynamics of this tRNA system, as will be described next.

Is tRNA dynamics comparable in the liquid and crystal phases?

X-ray structures are generally taken as starting points for MD simulations. As a criterion for estimating the quality of an MD simulation conducted in aquo, between experimental and calculated Debye-Waller or B-factors are often compared. However, intermolecular contacts and crystal packing effects are known to restrict the mobility range of the molecule in the crystal phase to an extent that is difficult to estimate. With the purpose of examining the validity of this criterion, the per-residue B-factors were calculated from the atomic fluctuations $\langle \delta r^2 \rangle^{1/2}$ according to the formula $B = (8\pi^2/3)\langle \delta r^2 \rangle$. The time dependence of the B-factors was

determined by calculating averages over different 100- and 500-ps time windows (Fig. 2).

As indicated by the B-factors calculated over the largest 500-ps time window (Fig. 2, *top*), the most mobile regions
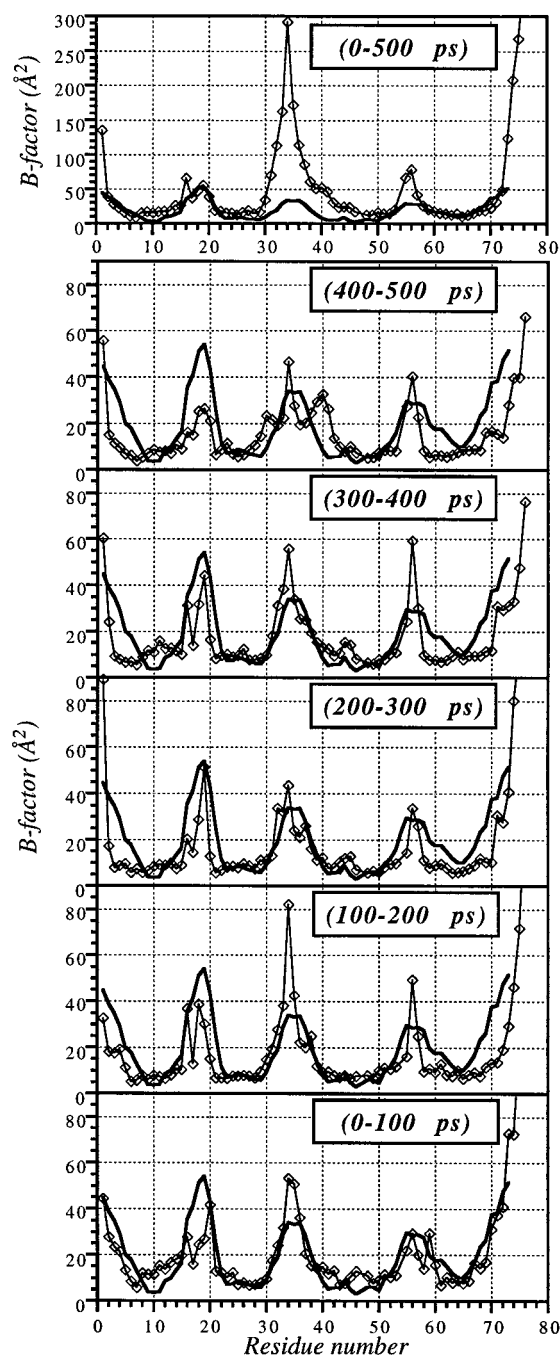

FIGURE 2   Per-residue B-factors for the entire tRNA calculated over different time windows. The solid lines correspond to the experimental B-factors, whereas the thin lines correspond to B-factors calculated from the MD simulation. To remove translational and rotational motions from simulation data and avoid artifacts associated with the inclusion in the fitting procedure of highly mobile regions (Hünenberger et al., 1995), the B-factors have been calculated from a trajectory in which each structure was superposed on the starting one. For the fitting procedure only the heavy atoms with experimental B-factors lower than 15 Å² (residues 6–15, 22–31, 39–53, and 61–67) were used.

of the L-shaped tRNA molecule are the anticodon loop and the acceptor stem extremity. The calculated B-factors of the 5′-U1 and 3′-CCA terminal residues as well as the apical G34 wobble nucleotide of the anticodon loop are especially high. The large mobility of the G34 nucleotide is consistent with the mobility calculated from previous MD simulations on the isolated tRNA^Asp anticodon hairpin fragment (Auffinger and Westhof, 1996). Yet the mobilities of the core residues remain fairly close to those derived from the crystal data. In particular, the residues of the D loop (14–21) display B-factors close to the experimental values, an exception being the D16 unpaired residue. Interestingly, for the TΨC loop, the residues Ψ55, C56, and A57 are more mobile in the MD than in the crystal. Interestingly, residues Ψ55, C56, and A57 of the TΨC loop are more mobile in the MD than in the solid phase. The lower mobility of these structural elements in the crystal may be related to the occurrence of intermolecular contacts. Among these are direct as well as water-mediated contacts involving residues of the acceptor stem, the D stem, the anticodon stem, and the TΨC loop. The most striking of these intermolecular contacts consists of the base pairs formed between the G34, U35, and C36 anticodon residues of symmetry-related molecules that mimic codon-anticodon interactions (Moras et al., 1980, 1986; Westhof et al., 1985). These interactions are not included in the dynamical model of the tRNA. It is worth noting that no low-frequency hinge-bending motions between the acceptor stem and the anticodon hairpin extremities were observed, and only a small pinch of the angle between the acceptor and anticodon arms (~5°) occurred, indicating that hinge-bending motions may occur only on nanosecond to microsecond time scales.

The convergence of the above-described B-factor was estimated by averaging their values over five successive 100-ps time windows (Fig. 2). The calculated per-residue B-factor profiles (see the *five bottom panels* of Fig. 2) change significantly with the selected time window. The best agreement between experimental and calculated B-factors occurs fortuitously for the 200–300-ps time window, with other time windows showing a variety of clearly noncorrelated profiles. It results that a 100-ps time window is too small to encompass the full dynamics of this tRNA molecule in solution. Similar conclusions have been drawn by Hünenberger et al. (1995) from nanosecond test simulations on two proteins: bovine pancreatic trypsin inhibitor and hen egg white lysozyme. The authors concluded that even B-factors calculated on a 500-ps time window are not converged and therefore do not give a reliable view of the absolute atomic motions of the system, although they describe reasonably well the mobility of the different domains of the proteins. Furthermore, they noted that, as the time window increases, the calculated B-factors increase and finally become significantly larger in the mobile regions than those derived from crystallographic experiments. Likewise, our results suggest that B-factors give a good picture of the global mobility of the tRNA molecule, although the calculated values are of qualitative character.

To get a sharper picture at the atomic level of the dynamical behavior of the different regions of the tRNA molecule, the behavior of the main tertiary interactions that sustain the fold of this complex tRNA architecture were analyzed in greater detail.

Stability of intramolecular hydrogen bonds

The dynamical stability of the standard and nonstandard base pairs is essential for maintaining the tertiary structure of a macromolecule and is certainly one of the best available criteria for estimating the quality of an MD trajectory. This stability has been evaluated by calculating hydrogen bonding percentages (HB%). These HB% are defined as the time over which a hydrogen bond satisfies the two $d(H\cdots O) < 2.5$ Å and $\theta(X\text{-}H\cdots O) < 135°$ standard criteria divided by the total simulation time (500 ps).

Stem base pairs

The base pairs forming the tRNA stems are well maintained during the 500 ps of the MD trajectory (Table 1). It is worth noting that the hydrogen bonds forming these base pairs display different levels of stability. The deep (major) groove side $(G)O_6\cdots H_{42}\text{-}N_4(C)$ hydrogen bond is the least stable in G-C base pairs (average HB% $\approx$ 72% over the 13 G-C stem base pairs). In contrast, the central $(G)N_1\text{-}H_1\cdots N_3(C)$ and shallow (minor) groove side $(G)N_2\text{-}H_{21}\cdots O_2(C)$ bonds display average HB% of 96% and 100%, respectively. These HB% values are in agreement with those derived from MD studies on smaller RNA fragments (Zichi, 1995; Auffinger and Westhof, 1996). The dynamical behavior of the closing m^5C49-G65 base pair of the TΨC stem, which stacks on the last A7-U66 base pair of the acceptor stem, is slightly different. The central and deep groove side hydrogen bonds are fairly stable while the $(m^5C49)H_{42}$ atom interacts with the O_6 atoms of residues G65 and G50 (Table 1). The formation of such a "bridged" interaction does not lead to a disruption of the base pair and may induce an additional stabilization of this region. However, from the MD results it is not possible to propose a role for the C49 methylation. Interestingly, the only modification detected for Cyt[49] is a methylation of the $(C)C_5$ atom, whereas no modifications of A, G, or U bases have been reported at this tRNA position (Sprinzl et al., 1998).

The three A-U base pairs (A7-U66, U11-A24, and U12-A23) are also well preserved. However, the first U1-A72 base pair of the acceptor stem opens partially during the simulation. Likewise, the hydrogen bonds of the three noncanonical G · U and analogous Ψ13 · G22 base pairs are conserved. As for G-C base pairs, the deep groove side hydrogen bond is, on the average, the most mobile (Table 1) (Zichi, 1995; Auffinger and Westhof, 1996).

Tertiary base pairs

Besides the stem base pairs, the extensive set of tertiary interactions present in tRNAs, which often involve phylo-

TABLE 1 Hydrogen bonding percentages (HB%) for tRNA stem base pair interactions

Base pairs	H-bonds	HB%
Acceptor stem		
U1–A72	$N_3\text{-}H_3\cdots N_1$	/
	$O_4\cdots H_{62}\text{-}N_6$	41
C2–G71	$N_4\text{-}H_{42}\cdots O_6$	88
	$N_3\cdots H_1\text{-}N_1$	96
	$O_2\cdots H_{21}\text{-}N_2$	100
C3–G70	$N_4\text{-}H_{42}\cdots O_6$	71
	$N_3\cdots H_1\text{-}N_1$	95
	$O_2\cdots H_{21}\text{-}N_2$	100
G4–C69	$O_6\cdots H_{42}\text{-}N_4$	66
	$N_1\text{-}H_1\cdots N_3$	97
	$N_2\text{-}H_{21}\cdots O_2$	100
U5 · G68	$N_3\text{-}H_3\cdots O_6$	76
	$O_2\cdots H_1\text{-}N_1$	97
G6–C67	$O_6\cdots H_{42}\text{-}N_4$	55
	$N_1\text{-}H_1\cdots N_3$	94
	$N_2\text{-}H_{21}\cdots O_2$	100
A7–U66	$N_1\cdots H_3\text{-}N_3$	98
	$N_6\text{-}H_{62}\cdots O_4$	44
D stem		
G10 · U25	$O_6\cdots H_3\text{-}N_3$	95
	$N_1\text{-}H_1\cdots O_2$	100
U11–A24	$N_3\text{-}H_3\cdots N_1$	70
	$O_4\cdots H_{62}\text{-}N_6$	89
U12–A23	$N_3\text{-}H_3\cdots N_1$	99
	$O_4\cdots H_{62}\text{-}N_6$	100
Ψ13 · G22	$N_3\text{-}H_3\cdots O_6$	99
	$O_4\cdots H_1\text{-}N_1$	96
Anticodon stem		
G27–C43	$O_6\cdots H_{42}\text{-}N_4$	76
	$N_1\text{-}H_1\cdots N_3$	95
	$N_2\text{-}H_{21}\cdots O_2$	99
G28–C42	$O_6\cdots H_{42}\text{-}N_4$	90
	$N_1\text{-}H_1\cdots N_3$	92
	$N_2\text{-}H_{21}\cdots O_2$	100
C29–G41	$N_4\text{-}H_{42}\cdots O_6$	62
	$N_3\cdots H_1\text{-}N_1$	97
	$O_2\cdots H_{21}\text{-}N_2$	99
G30 · U40	$O_6\cdots H_3\text{-}N_3$	70
	$N_1\text{-}H_1\cdots O_2$	97
C31–G39	$N_4\text{-}H_{42}\cdots O_6$	69
	$N_3\cdots H_1\text{-}N_1$	87
	$O_2\cdots H_{21}\text{-}N_2$	98
TΨC stem		
m^5C49–G65	$N_4\text{-}H_{42}\cdots O_6$	27
	$N_3\cdots H_1\text{-}N_1$	93
	$O_2\cdots H_{21}\text{-}N_2$	99
G50–C64	$O_6\cdots H_{42}\text{-}N_4$	84
	$N_1\text{-}H_1\cdots N_3$	99
	$N_2\text{-}H_{21}\cdots O_2$	100
G51–C63	$O_6\cdots H_{42}\text{-}N_4$	89
	$N_1\text{-}H_1\cdots N_3$	100
	$N_2\text{-}H_{21}\cdots O_2$	100
G52–C62	$O_6\cdots H_{42}\text{-}N_4$	77
	$N_1\text{-}H_1\cdots N_3$	100
	$N_2\text{-}H_{21}\cdots O_2$	100
G53–C61	$O_6\cdots H_{42}\text{-}N_4$	82
	$N_1\text{-}H_1\cdots N_3$	100
	$N_2\text{-}H_{21}\cdots O_2$	99

genetically conserved bases, is essential for maintaining their complex three-dimensional fold (Quigley and Rich, 1976; Saenger, 1984). In yeast tRNA^{Asp}, four non-Watson-Crick tertiary base pairs are present (Westhof et al., 1985): the *trans* Hoogsteen T54 · A58, essential for the structure of the TΨC loop; the *trans* Hoogsteen U8 · A14; the *trans* Watson-Crick A15 · U48; and the *cis* Watson-Crick G26 · A44 base pairs. In the A form of yeast tRNA^{Asp} investigated in the present study, an additional tertiary contact involves the Watson-Crick G18-C56 base pair (see Fig. 1; in the crystal, G18-C56 is stacked over the same base pair of a symmetry-related molecule; Westhof et al., 1988). The pronounced stability of the G18-C56 interaction linking the D and T loops is surprising because its absence is the main difference between the two known A and B crystal forms analyzed by x-ray crystallography (Moras et al., 1980). Furthermore, it is worth noting that during the MD simulation, all of the tertiary interactions display stabilities comparable to those of the Watson-Crick stem base pairs (Fig. 3 and Table 1).

Several single interbase hydrogen bonds are also observed. Across the anticodon loop, Ψ32 · C38 forms a single "bifurcated" tertiary hydrogen bond that is preserved along the 500 ps of MD, as also noted in preceding MD simulations of the anticodon hairpin (Auffinger and Westhof, 1996, 1997a, 1998a). Likewise, the single $(G17)N_1$-H_1···O_4(Ψ55) tertiary bond that links the D to the TΨC loop (Fig. 1 *A*) displays an HB% of 85%. However, the $(Ψ55)O_4$ atom shows a strong tendency to form bifurcated hydrogen bonds with the H_1 and H_{21} atoms of G17 rather than a single linear hydrogen bond to the H_1 atom (Fig. 3). Such a bifurcated hydrogen bonding pattern has also been reported for the analogous interaction between G18 and Ψ55 in yeast tRNA^{Phe} (Quigley and Rich, 1976). Similar bifurcated interactions have been observed in the loop E of 5S rRNA by NMR (Dallas and Moore, 1998) and by crystallography (Correll et al., 1997) between G102 and U74 as well as between G100 and G76.

Base triples

Four base triples are located in the core of the tRNA, i.e., A21···[U8 · A14], A46···[Ψ13 · G22], A9···[U12-A23], and G45···[G10 · U25]. The Watson-Crick U12-A23 and as well as the wobble G10 · U25 and Ψ13 · G22 base pairs belong to the D stem and form stable hydrogen bonds (Table 1). Likewise, the tertiary *trans* Hoogsteen U8 · A14 base pair displays similar stability (Fig. 3). On the other hand, the interactions involving the third base of the triples are found, in each case, to be less stable (Fig. 4).

The G45···[G10 · U25] triple (in *red* in Figs. 1 *A* and 6), which contributes to the interaction of the variable loop with the D stem, remains planar during the MD simulation. However, there is a marked tendency for G45 to slide toward U25 to form a $(U25)O_4$···H_{21}-N_2(G45) hydrogen bond with a $(G10)O_6$···$H_{(1/2)}$-N_2(G45) bifurcated interaction
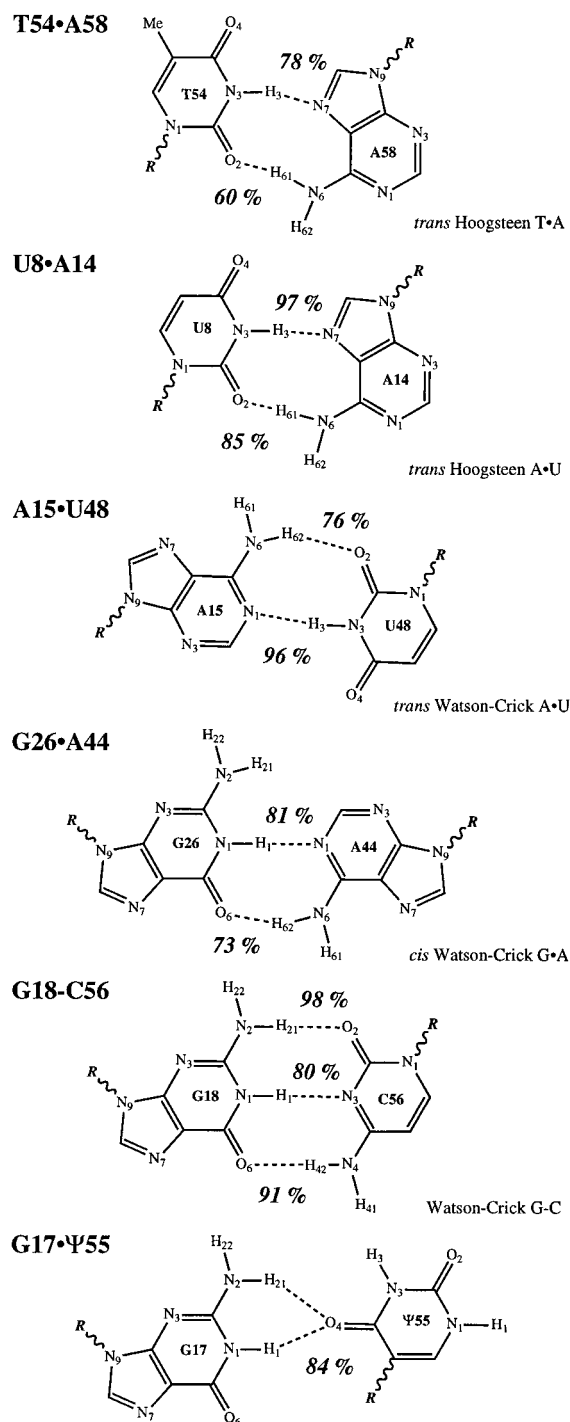

FIGURE 3   HB% calculated from the 500-ps MD simulation for the five tertiary base pairs present in yeast tRNA^{Asp} and the G17 · Ψ55 interaction linking the D and TΨC loops.

at the expense of the $(G10)N_7$···H_{22}-N_2(G45) hydrogen bond (Fig. 5). During the simulation, these hydrogen bonding patterns exchange a few times and suggest a possible dynamical equilibrium.

In the core of the tRNA, the A21···[U8 · A14], A46···[Ψ13 · G22], and A9···[U12-A23] base triple lose
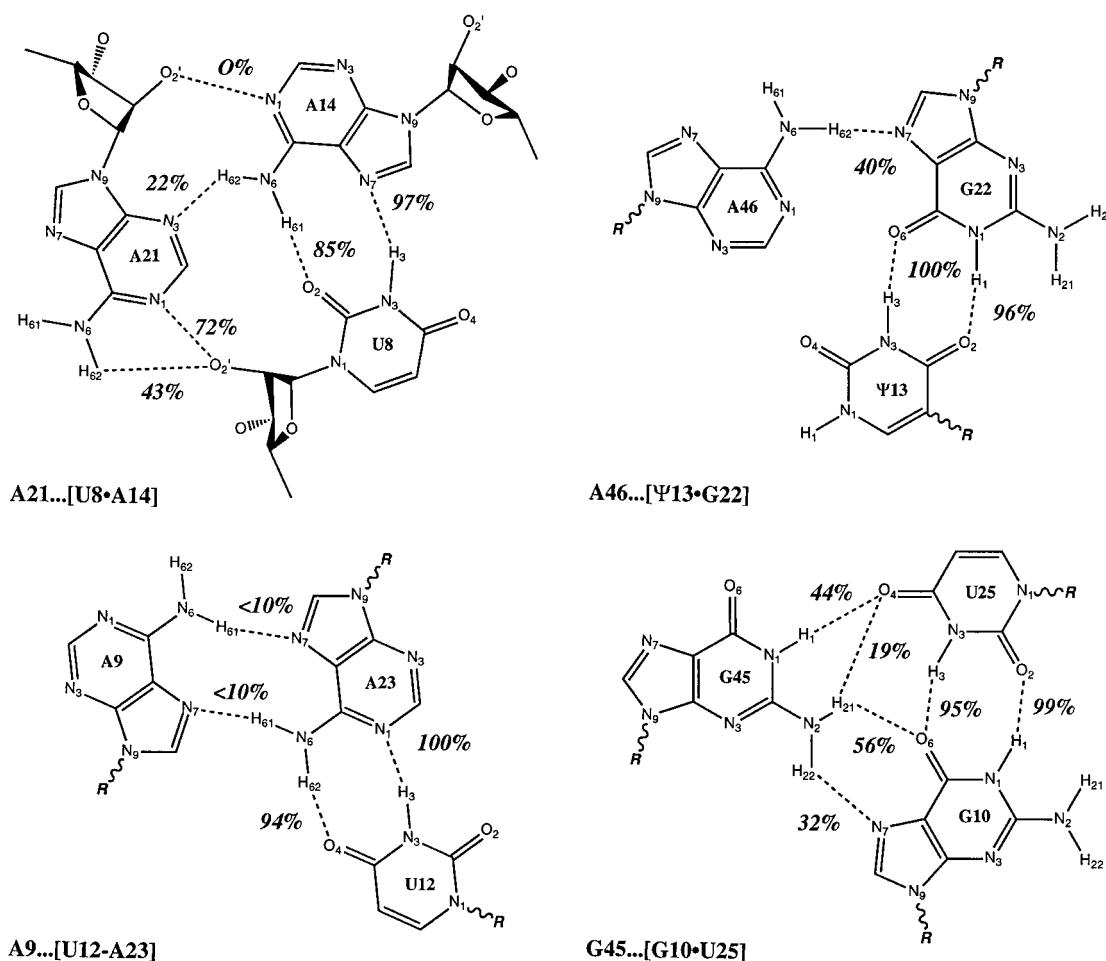
FIGURE 4   HB% calculated from the 500-ps MD simulation for the base triples observed in the crystal structure of yeast tRNA^{Asp}.

their coplanarity during the simulation as a result of a shift of the bases located in the deep groove of the D stem (Fig. 6). A loss of the interaction between A9 and the U12-A23 base pair (in *blue* in Figs. 1 *A* and 6) occurs almost immediately at the start of the simulation. The hydrogen bonds between A9 with A23 seen in the crystal structure break and A9 instead establishes a triple interaction with the U11-A24 base pair (in *cyan* in Figs. 1 *A* and 6). This "new" triple is characterized by a bifurcated (A9)N$_7$···N$_6$(A24) hydrogen bond. After this displacement, the A46 base shifts from the deep groove of the Ψ13 · G22 base pair (in *yellow* in Figs. 1 *A* and 6) toward the U12-A23 base pair and forms the (A46)N$_6$···N$_7$(A23) and (A46)N$_1$···N$_6$(A23) hydrogen bonds. Finally, the A21 base of the last triple (in *green* in Figs. 1 *A* and 6), which does not form stable hydrogen bonds with the U8 · A14 *trans* Hoogsteen base pair, shifts slightly toward the Ψ13 · G22 base pair without forming new hydrogen bonding contacts.

This cooperative rearrangement of the base triples in the tRNA core is the most significant structural event observed for any set of interactions during the simulation. It suggests that the triple interactions observed in the crystal structure are not as stable as the Watson-Crick and noncanonical base

pairs and point to a possible structural heterogeneity or polymorphism inherent to base triples. In several tRNAs, different triple interactions are observed. For example, in yeast tRNA^{Phe} (Quigley and Rich, 1976), which contains the extra base 47 in the variable loop, A9 interacts with A23 and forms an additional (A9)N$_6$-H$_{62}$···O$_R$(A23) hydrogen bond not present in yeast tRNA^{Asp} (Westhof and Sundaralingam, 1986). A Mg^{2+} binding site close to the phosphate of residue A9 in the crystal structure of tRNA^{Phe} (Jack et al., 1977) and the presence of an analogous peak assigned to a water molecule in tRNA^{Asp} (a position occupied by a gadolinium ion in heavy atom replacement) may account for the differences. Thus the tertiary interaction pattern may be dependent on the ionic environment of the tRNA and on the presence of Mg^{2+} ions. This correlates well with experimental data indicating that divalent ions are essential for correct folding of RNA molecules (for a review, see Brion and Westhof, 1997). Given the particular geometry of the A46···[Ψ13 · G22] triple observed in the crystal structure (Westhof et al., 1985), a protonation of base A46 would also lead to the stabilization of this base triple. This possibility is strengthened by the fact that a large number of charged m^{7}G (m^{7}G)$^{+1}$ residues are found at position 46 of tRNAs
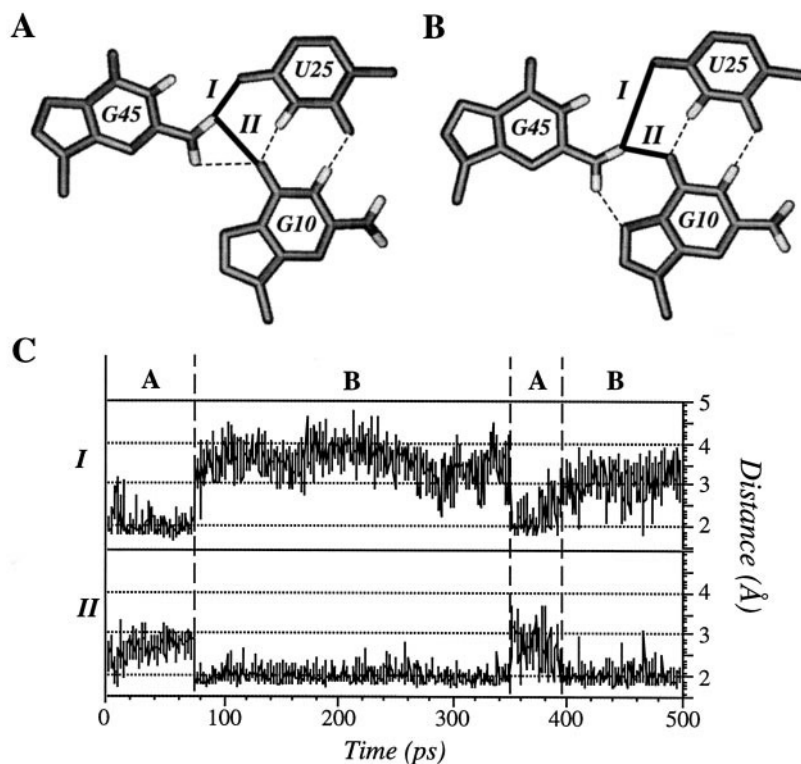
FIGURE 5   (*A*) Hydrogen-bonding patterns observed for the G45···[G10 · U25] base triple in the crystal and (*B*) during the MD simulation (see also Fig. 4). (*C*) Time course of the distance of the possible $(G45)N_2–H_{21}···O_4(U25)$ hydrogen bond (I) and $(G45)N_2-H_{21}···O_6(G10)$ hydrogen bond (II). The plot of hydrogen bond interactions monitors the exchange process of the hydrogen bonding patterns shown in *A* and *B*.

(Sprinzl et al., 1998). However, there is no direct experimental evidence concerning the status of the protonation state of base A46 in yeast tRNA^{Asp}. Further simulation studies might help in this matter.

Among the triple interactions located in the tRNA^{Asp} core, the A21···[U8 · A14] triple involves, besides base-base interactions, two sugar-base hydrogen bonds, i.e., $(U8)O_{2'}-H···N_1(A21)$ and $(A14)N_1···H-O_{2'}(A21)$ (see Fig. 4). As discussed above, the tertiary interactions between U8 and A14 are well preserved, whereas the $(A14)N_6-H_{62}···N_3(A21)$ interaction is relatively unstable (average distance of 2.7 Å; HB% ≈ 22%). The base-sugar $(U8)O_{2'}-H···N_1(A21)$ interaction, after displaying high fluctuations during the initial 100 ps, settles into a standard hydrogen bond geometry for the remainder of the trajectory (HB% ≈ 72%; see Figs. 4 and 7). However, the base-sugar $(A14)N_1···H-O_{2'}(A21)$ interaction is not formed during the simulation (average distance of 5.7 Å). It is interesting that the most stable hydrogen bond involving a hydroxyl group (i.e., $(U8)O_{2'}-H···N_1(A21)$) is also proposed to occur in the tRNA^{Phe} structure (Quigley and Rich, 1976).

Base-backbone interactions

In the crystal structure, two base-backbone interactions involving the invariant U33 and Ψ55 residues maintain the U-turns of the anticodon and TΨC loops. The $(U33)N_3-H···O_R(U35)$ hydrogen bond across the anticodon loop is especially well conserved (HB% of 100%), as observed in other simulations of the anticodon loop (Auffinger et al., 1996b; Auffinger and Westhof, 1996). However, the anal-

ogous $(Ψ55)N_3-H···O_R(A58)$ interaction across the thymine loop (see Fig. 1 *A*) breaks after ~100 ps (HB% close to 17%) due to dynamical rearrangements. Leroy et al. (1985) reported that the lifetime of the $(Ψ55)N_3-H···O_R(A58)$ bond, which is close to 20 ms at 27°C in the absence of Mg^{2+} ions, increases to more than 100 ms in a buffer that contains 10 Mg^{2+} ions per tRNA molecule. Similar results have been obtained for tRNA^{Gly} (Amano and Kawakami, 1992), which indicate that the TΨC region is particularly sensitive to the presence of Mg^{2+} ions. In contrast, the U-turn of the anticodon loop seems to be less sensitive to the presence of divalent ions.

It is worth noting that only a subset of the short intramolecular contacts identified in the crystal structure (Westhof et al., 1985) led to dynamically stable hydrogen bonds during the 500-ps MD simulation. In the TΨC loop, the HB% of the $(U60)O_S···H_{41}-N_4(C61)$ contact (crystal structure N···O distance 2.9 Å) is close to 75%. Just adjacent, a $(G18)O_S···H-N_3(U60)$ hydrogen bond not present in the crystal structure is formed during the MD run (HB% ≈ 89%). As discussed above, base-backbone interactions also contribute to some extent to the A21···[U8 · A14] base triple (Fig. 4). Among the intramolecular contacts that do not lead to stable hydrogen bonds during the simulation are some hydrogen bonding contacts in base triples discussed above, the $(G18)N_2···O_R(A21)$ and $(A9)O_{2'}···N_7(G10)$ contacts, as well as several contacts involving the $O_{2'}$ atoms of the ribose groups.

C-H···O interactions are now recurrently found in biomolecules (Derewenda et al., 1995; Steiner, 1996; Auffinger and Westhof, 1997b; Wahl and Sundaralingam, 1997) and

FIGURE 6 (*Top and middle*) Stereo views displaying the residues constituting the structural core of the tRNA molecule (the color code is the same as the one used in Fig. 1 *A*). The stereo view shown in the top panel is extracted from the crystal structure; the stereo view shown in the middle panel is extracted from the last structure of the MD simulation. (*Bottom*) Two sketches of the structural arrangement observed before and after the 500 ps of MD simulation. The slippage of the three central base triples (A21···[U8 · A14]; A46···[Ψ13 · G22]; A9···[U12-A23]) sandwiched between A15 · U48 and G45···[G10 · U25] and following an opening of the P10 loop is clearly visible.
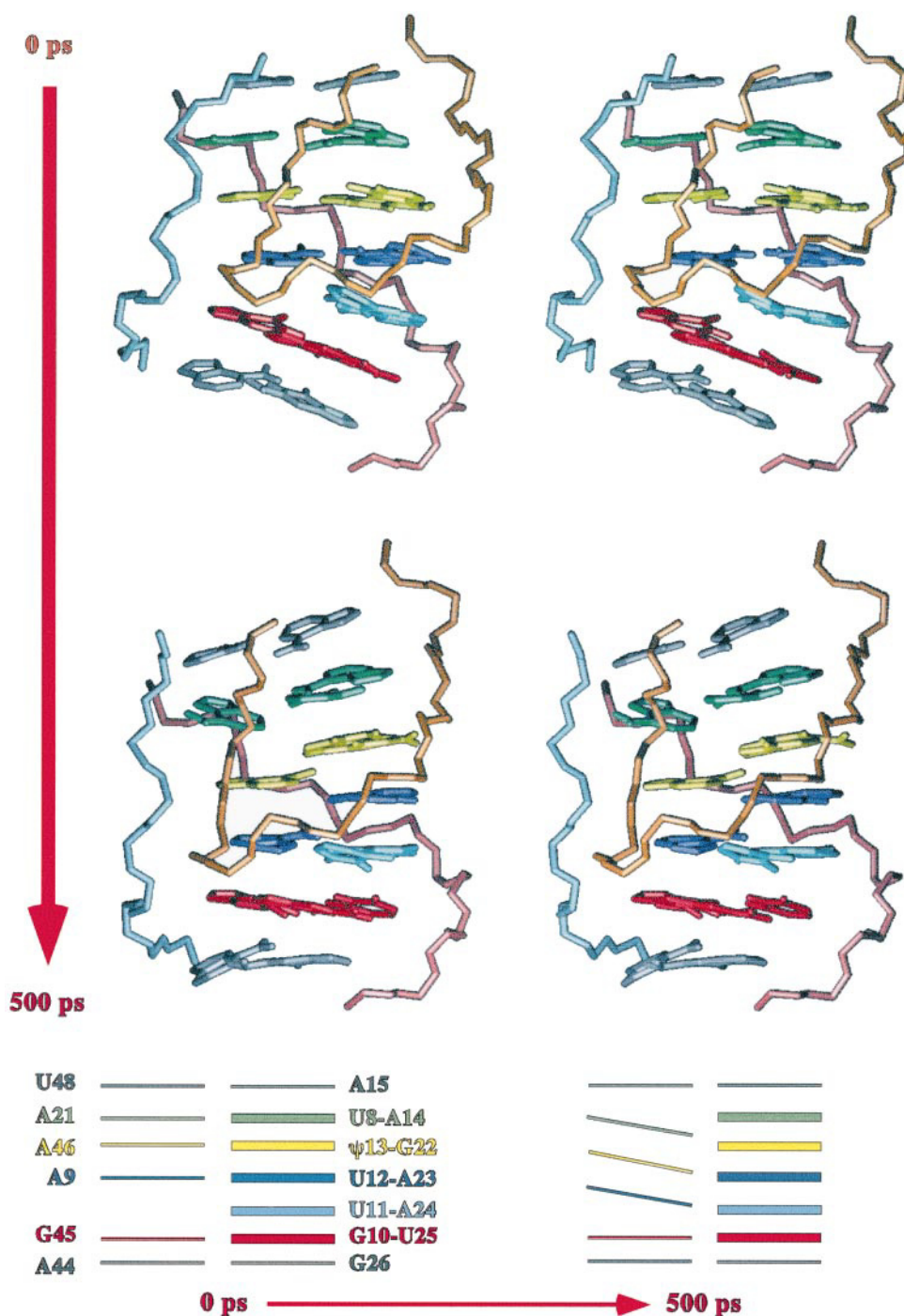
have been shown to possess specific structural as well as functional roles. In nucleic acids, besides the well-known $C_{6/8}$-H···$O_{5'}$ interactions, linking the base to the backbone and stabilizing the preferred conformations of nucleotides (Saenger, 1984), two C-H···O interactions have been found to contribute to the stability of the tRNA^{Asp} anticodon loop, i.e., (U35)C_5-H···$O_{2'}$(U33) and (C36)C_5-H···O_2(U33). These C-H···O interactions were first characterized from MD simulations on the isolated tRNA^{Asp} anticodon hairpin (Auffinger et al., 1996b; Auffinger and Westhof, 1996, 1998a) and are found to be stable in the MD simulation of the entire

tRNA molecule, validating to some extent the conclusions drawn from studies on isolated fragments.

Backbone-backbone interactions

In RNA, the only possible backbone-backbone interactions between hydrophilic atoms involve the unique hydrogen bond donor 2′-hydroxyl group of the sugar. This 2′-hydroxyl group can potentially form hydrogen bonds with the anionic O_R, O_S, $O_{3'}$, and $O_{5'}$ phosphate oxygens, the ribose
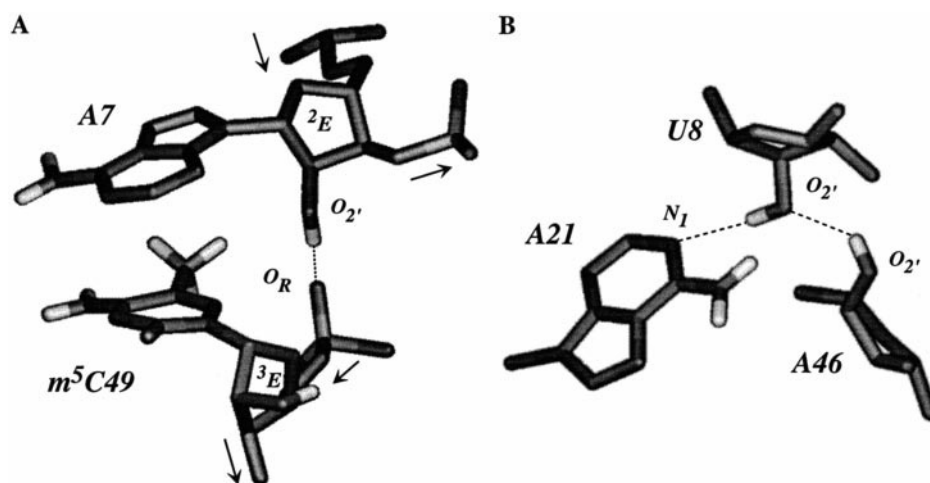
FIGURE 7 (*A*) Backbone-backbone interaction involving the hydroxyl group of the A7 sugar (last residue of the 5′ strand of the acceptor stem), which is in a $C_{2'}$-*endo* (2_E) conformation with the O_R atom of the methylated cytosine 49 (first residue of the 5′ strand of the TΨC stem). This interaction, which is stable during the 500 ps of MD simulation, might contribute to the stabilization of the right-handed stack between the acceptor and TΨC helices. The arrows mark the 5′-to-3′ direction. (*B*) Stable ribose-ribose motif observed during the 500 ps of MD simulations. The hydroxyl groups of both U8 and A46 residues point toward their "base" domain (Auffinger and Westhof, 1997b), so that (U8)$O_{2'}$ donates its proton to (A21)N_1 while receiving a hydrogen bond from (A46)$O_{2'}$.

$O_{4'}$ atoms, or the $O_{2'}$ atom of other 2′-hydroxyl groups, like those ribose zipper motifs (Berger and Egli, 1997). Stereochemical rules describing the possible and forbidden orientations of the 2′-OH group for sugars in the $C_{3'}$- and $C_{2'}$-*endo* puckers have recently been derived from MD simulations of tRNA fragments (Auffinger and Westhof, 1997b).

Yet, as inferred early from the crystal structures structure of yeast tRNA^{Phe} (see Quigley and Rich, 1976), the 2′-OH group makes significant hydrogen bonding contacts in the nonhelical regions. In the present simulation, two stable hydrogen bonds between a 2′-hydroxyl group and an anionic phosphate oxygen atom have been identified, i.e., (A7)$O_{2'}$-H···O_R(m^{5}C49) (HB% ≈ 99%) (see Fig. 7 *A*) and (D16)$O_{2'}$-H···O_S(C61) (HB% ≈ 71%). Interestingly, the sugars of both residues A7 and D16 adopt the unusual $C_{2'}$-*endo* pucker. Furthermore, a long-lived hydroxyl-hydroxyl interaction between U8 and A46 is formed (Fig. 7 *B*; see also figure 4 in Auffinger and Westhof, 1997b). The 2′-OH group of U8 is in turn involved in a stable interaction with the N_1 atom of A21 (Figs. 4 and 7 *A*). Both of these hydroxyl groups are pointing toward the conformational allowed "base" domain (Auffinger and Westhof, 1997b). This motif is reminiscent of the ribose zipper motif, which plays a significant role in numerous inter- and intramolecular RNA-RNA interactions (Dock-Bregeon et al., 1989; Schindelin et al., 1995; Cate et al., 1996; Berger and Egli, 1997).

More surprisingly, the $O_{2'}$-H(n)···$O_{4'}$($n + 1$) hydrogen bond, which was often proposed to contribute to the stabilization of RNA helical conformations (Saenger, 1984; Jeffrey and Saenger, 1991), is not observed in the MD simulations. It has been proposed, in agreement with crystallographic data, that recurrent intrastrand C-H···O hydrogen bonds, i.e., $C_{2'}$-H(n)···$O_{4'}$($n + 1$) interactions, may contribute to the stabilization of RNA helical structures in the axial direction, whereas the 2′-OH groups prefer to form hydrogen bonds with water molecules (Auffinger and Westhof, 1997b).

DISCUSSION

The present 500-ps MD simulation of the 75-nucleotide yeast tRNA^{Asp} molecule reveals a good overall preservation of most of the important interactions contributing to the stability of its molecular architecture. Among these, the stem and tertiary base pairs are well maintained during the MD trajectory (Table 1 and Fig. 3). This represents considerable progress with respect to early nucleic acid MD simulations, in which unphysical breaking events of base pairs were reported on short (100 ps) time vscales for DNA duplexes (Louise-May et al., 1996; Beveridge et al., 1997; Auffinger and Westhof, 1998b). As such, the present MD simulation has been used to determine that, because of an improved treatment of the long-range electrostatic forces through the use of the particle mesh Ewald (PME) method, it is now possible to perform accurate MD simulations of complex folded nucleic acid molecules similar in size to small proteins.

tRNA mobility in solution and in the crystal

The mobilities of the different parts of the tRNA have been estimated through the comparison of experimental and calculated B-factors. Whereas the calculated mobilities of the acceptor and anticodon extremities of the L-shaped tRNA molecule are larger than those observed in the crystal, the

mobilities of the core residues are found to be of the same order of magnitude in the aqueous and crystalline environment. This result indicates that, in restrained regions characterized by dense packing of residues involving numerous tertiary hydrogen bonds, there is no appreciable difference between the estimated solution and crystal B-factors. In peripheral regions that are mainly involved in crystal packing interactions, like the acceptor and anticodon extremities, the atomic mobilities in the solid and liquid phases differ considerably. As expected, the mobilities of the tRNA extremities are the largest in solution. Thus calculated B-factors give a realistic picture of the relative mobility of the different domains of the simulated molecule in an aqueous environment.

From a methodological point of view, the present results make clear that a direct comparison between calculated and experimental B-factors is not generally a useful criterion for assessing the quality of an MD trajectory (Hünenberger et al., 1995) unless the simulation includes an explicit representation of the crystal environment (Lee et al., 1995a,b; York et al., 1995). They also point to the necessity of performing careful checks of the convergence of these B-factors on different time windows before interpretation. Such convergence checks give a sense of the reliability of the calculated data as well as a rough estimate of the relaxation time scale of the simulated processes.

tRNA structural stability in solution

As stated above, the standard and nonstandard base pairs are well maintained during the 500 ps of the simulation. This is a very satisfying result, as NMR studies indicate that stem base pair breaking events occur on much longer microsecond to millisecond time scales (Leroy et al., 1985; Kochoyan et al., 1990; Moe and Russu, 1990). Interestingly, the five tertiary base pairs of yeast tRNA^{Asp} were also found to be stable during the MD simulation (Fig. 3). In agreement with this result, NMR investigations of various tRNA molecules have shown that tertiary base pairs exhibit lifetimes in the millisecond range, even in the absence of Mg^{2+} ions (Leroy et al., 1985). Likewise, other studies have shown that NMR resonances associated with tertiary base pairs can be detected in various tRNAs under different ionic conditions and temperatures (Kintanar et al., 1994; Choi and Redfield, 1995).

However, given the size of the tRNA molecule, base triples are difficult to assign unambiguously by NMR methods (Choi and Redfield, 1985, 1986; Hyde and Reid, 1985a; Hall et al., 1989; Amano and Kawakami, 1992), and no data are available on their lifetimes. The experimental difficulties involved in the detection of base triples in solution may be partly related to a greater lability of these interactions. Such a lability is observed in the MD trajectory, where the interactions of bases located in the deep groove of secondary or tertiary base pairs were found to display different levels of stability, going from an apparently reversible ex-

change of hydrogen bond patterns for the G45···[G10 · U25] triple (Fig. 5) to a complete loss of interactions of the three other base triples (Fig. 6), which results in a cooperative slide of the deep groove bases. The above structural rearrangement is made possible by the fact that the U11-A24 base pair of the D stem does not participate in a triple interaction, thereby introducing a break in the stack of the four base triples (Fig. 6).

On the other hand, the lability of several tertiary interactions observed in the MD simulation, in the base triples but also in the U-turn in the TΨC loop, may be related to the absence of Mg^{2+} ions in the model (the present MD simulation has been conducted in the absence of Mg^{2+} ions because none were detected by crystallography; Westhof et al., 1985). The fact that the tertiary structure of RNA molecules and especially tRNAs are particularly sensitive to the presence of Mg^{2+} ions is well appreciated (for a review, see Brion and Westhof, 1997). A large number of studies have reported a significant sensitivity of the tRNA three-dimensional architecture to the presence of Mg^{2+} ions (Heerschap et al., 1982; Hyde and Reid, 1985b; Hall et al., 1989; Perret et al., 1990; Reid and Cowan, 1990; Amano and Kawakami, 1992; Kintanar et al., 1994; Yue et al., 1994; Choi and Redfield, 1995; Serebrov et al., 1998). Early works by Stein and Crothers (1976a,b) have pinpointed the central role of the triples in the D stem for the kinetics of tRNA folding. These authors have shown that the triple-helical scaffold constitutes a folding nucleus and that its formation 1) constitutes the rate-limiting step in tertiary structure formation and 2) creates binding sites for Mg^{2+} ions. Heerschap et al. (1982) noted that yeast tRNA^{Phe} adopts in a 5 mM solution of Mg^{2+} ions a conformation different from that observed in an excess of 320 mM of Na$^+$ ions. Hall et al. (1989) noted observed shifts in the U8 · A14 and (Ψ55)N$_1$-H resonances of a solution of yeast tRNA^{Phe} in 0.1 M NaCl when Mg^{2+} is added. Other authors have reported that four strong Mg^{2+}-binding sites must be occupied to stabilize the tRNA tertiary structure (Reid and Cowan, 1990; Amano and Kawakami, 1992; Choi and Redfield, 1995). Amano and Kawakami (1992) reported that NMR peak shifts were the largest for resonances associated with the T54 · m^{1}A58 and Ψ55(H$_1$) (Ψ55)N$_1$-H imino protons and affected the resonances of the D and TΨC loops, the G15-m^{5}C48, the U8 · A14, and the D stem base pairs of the *Bombyx mori* tRNA^{Gly}. They proposed that strong Mg^{2+}-binding sites are located near the D stem, and U8 · A14 and the tertiary base pairs between the D and TΨC loops. These binding sites are supposed to be the same or close to those that have been described in the yeast tRNA^{Phe} crystal structure (Jack et al., 1977). Yue et al. (1994) have also observed a disruption of the D stem and a loss of tertiary interactions at low Mg^{2+} concentration for an in vitro transcribed *E. coli* tRNA^{Val} molecule. Early works by Stein and Crothers (1976a,b) have pinpointed the important role of the D stem in the kinetics of tRNA folding. These authors have shown that the D helix constitutes a folding nucleus and that its formation 1) constitutes the

rate-limiting step in tertiary structure formation and 2) creates binding sites for Mg^{2+} ions.

Recently, Friederich et al. (1998) have used a transient electronic birefringence method to characterize the flexibility of the tRNA^Phe core. They concluded that in the presence of magnesium ions the global flexibility of the tRNA core is not significantly greater than the flexibility of RNA helices, whereas in the absence of magnesium ions the core becomes quite flexible under conditions were the secondary structure elements are intact. As in our conclusions, they speculated that the higher mobility of the tRNA may be due to the absence of magnesium ions in the 8–12 turn and between the D and T loops.

Thus the absence of Mg^{2+} ions in our model may account for the structural rearrangement described above. Hence the MD trajectory may give some insight into conformational transitions occurring when structurally important Mg^{2+} ions are missing. The interpretation of Mg^{2+}-related structural transitions may be of importance, as it has recently been shown that the cognate synthetase of *E. coli* tRNA^Phe interacts with different identity elements of the tRNA, depending on low or high Mg^{2+} concentrations, which suggests that the conformation of the tRNA recognized by the protein is different in the two environments (Kholod et al., 1997). Clearly, simulations including magnesium ions should be performed. However, this is made difficult by the absence of evidence of magnesium ion binding sites in the yeast tRNA^Asp crystal structure (Westhof et al., 1985).

In addition, the observed lability of the base triples in the tRNA core points to a structural heterogeneity involving these tertiary interactions. Such a heterogeneity may be related to the difficulties encountered in localizing triple interactions from comparative sequence analysis in RNA molecules (Gautheret et al., 1995; Gautheret and Gutell, 1997). The absence of strict constraints between bases forming triple interactions may be mandatory for allowing the formation of various (and almost isosteric) interaction schemes observed in the core of known tRNA molecules (Gautheret et al., 1995; Masquida and Westhof, 1998). The absence of stringent hydrogen bonding rules may also lead to an additional requirement for Mg^{2+} binding to achieve adequate stability of the RNA fold. In folded RNAs, it is indeed often observed that destabilizing mutations can be rescued by an increase in the concentration of Mg^{2+} ions. Alternatively, mutations in base triples may lead to a weakening of the binding of a nearby Mg^{2+} ion and perturb the structure of the tRNA core. For example, Hou (1994) noted that mutations in the tRNA triples 21···[8–14] and 46···[13–22] had major effects on the 15–48 base pair, indicating the existence of large physical constraints in the tRNA core.

Besides base-base interactions, several tertiary contacts involving the ribose 2′-OH groups were identified in the crystal structure of yeast tRNA^Asp (Westhof et al., 1985) and yeast tRNA^Phe (Quigley and Rich, 1976; Westhof and Sundaralingam, 1986). Such interactions were shown, by substitution experiments of wild-type residues by deoxyribose nucleotides, to play a significant role in the preservation of the tRNA tertiary structure (Aphasizhev et al., 1997). In the simulation, these interactions display different levels of stability and were observed to be among the most versatile tertiary contacts. Similar conclusions were drawn from MD simulations of the hammerhead ribozyme (Hermann et al., 1998).

Finally, we would like to address the question of the length of the simulation, which is "relatively" short (500 ps) compared to the five nanosecond simulations on DNA duplexes that have recently been published (Feig and Pettitt, 1997; Young et al., 1997; Young and Beveridge, 1998). A first remark concerns the respective size and complexity of the investigated system, which is obviously different in the two cases. More significantly, we have a restricted knowledge of the dynamics of tRNA molecules and the structural transitions that may occur on picosecond to nanosecond or microsecond time-scales because of intrinsic or environmental factors, such as the strength and nature of the ionic atmosphere. In the present study, we noted a relatively important structural rearrangement involving base triples that occurred in the core of the tRNA molecule on the 500-ps time scale, likely resulting from the absence of structurally important magnesium ions. Besides obvious CPU time limitations, it seemed more appropriate to analyze in detail the present structural transitions instead of extending the length of the simulation, because they lead to a deviation from the crystallographic structure, still the best picture we have of the conformation of an active yeast tRNA^Asp molecule. It is unlikely that longer simulations would have given a clearer understanding of the factors at the origin of this transition. Instead, the present work will be used as a basis for subsequent and longer simulations investigating environmental effects with the aim of outlining the factors affecting the stability of the tRNA core.

CONCLUSIONS

Transfer RNA molecules participate in various biological processes beyond protein synthesis. All of these processes involve specific interactions with proteins or ribosomal RNAs and imply elaborate recognition features. tRNAs retain their complex three-dimensional fold through tertiary interactions involving phylogenetically conserved bases. Therefore, it is of particular importance to understand at the atomic level the rules governing the stability of these complex three-dimensional folds. Indeed, the understanding of these rules proceeds from our ability to reproduce the dynamical behavior of these molecules. The present MD simulation constitutes a step toward this goal. In contrast to early MD simulations of RNA molecules, most of the tertiary interactions present in the reference yeast tRNA^Asp crystal structures were maintained during the 500 ps of the MD simulation after an accurate treatment of the long-range electrostatic interactions through the use of the particle mesh Ewald method. This result is of significance, as it shows that it is now possible to accurately simulate highly

Biophysical Journal Volume 76 January 1999

charged RNA molecules of the size of small proteins on time scales reaching the nanosecond.

It is well appreciated that Mg^{2+} ions are essential for folding tRNAs in their active conformation and that tRNAs undergo several structural rearrangements in tertiary structure when they are deprived of magnesium ions. However, no experimental data are available describing at the atomic level these magnesium-induced structural transitions. In the MD simulation, a structural rearrangement in the core of the tRNA molecule, where all of the base triples cluster, was observed. This rearrangement revealed a greater lability of base triples compared to secondary and tertiary base pairs. Thus it was inferred, in agreement with experimental results, that Mg^{2+} ions play an essential role in the stabilization of the tRNA core. Simulations of tRNA molecules in aqueous solutions at different Mg^{2+} concentrations will help to precisely define the structural impact of divalent ions. Such simulations will benefit from the rapid evolution of computer power and MD algorithms. Yet the present simulation gives some interesting insights into structural rearrangements that may occur in a neutral aqueous environment in the absence of divalent ions.

REFERENCES

Amano, M., and M. Kawakami. 1992. Assignment of the magnetic resonances of the imino protons and methyl protons of *Bombyx mori* tRNA^{Gly}(GCC) and the effect of ion binding on its structure. *Eur. J. Biochem.* 210:671–681.

Aphasizhev, R., A. Théobald-Dietrich, D. Kostyuk, S. N. Kochetkov, L. Kisselev, R. Giegé, and F. Fasiolo. 1997. Structure and aminoacylation capacities of tRNA transcripts containing deoxyribonucleotides. *RNA.* 3:893–904.

Auffinger, P., S. Louise-May, and E. Westhof. 1996a. Hydration of C-H groups in tRNA. *Faraday Discuss.* 103:151–174.

Auffinger, P., S. Louise-May, and E. Westhof. 1996b. Molecular dynamics simulations of the anticodon hairpin of tRNA^{Asp}: structuring effects of C-H⋯O hydrogen bonds and of long-range hydration forces. *J. Am. Chem. Soc.* 118:1181–1189.

Auffinger, P., and E. Westhof. 1996. H-bond stability in the tRNA^{Asp} anticodon hairpin: 3 ns of multiple molecular dynamics simulations. *Biophys. J.* 71:940–954.

Auffinger, P., and E. Westhof. 1997a. RNA hydration: three nanoseconds of multiple molecular dynamics simulations of the solvated tRNA^{Asp} anticodon hairpin. *J. Mol. Biol.* 269:326–341.

Auffinger, P., and E. Westhof. 1997b. Rules governing the orientation of the 2′-hydroxyl group in RNA. *J. Mol. Biol.* 274:54–63.

Auffinger, P., and E. Westhof. 1998a. Effects of pseudouridylation on tRNA hydration and dynamics: a theoretical approach. *In* Modification and Editing of RNA. H. Grosjean and R. Benne, editors. American Society for Microbiology, Washington, DC. 103–112.

Auffinger, P., and E. Westhof. 1998b. Molecular dynamics of nucleic acids. *In* Encyclopedia of Computational Chemistry. P. v. R. Schleyer, editor. Wiley and Sons, New York.

Auffinger, P., and E. Westhof. 1998c. Simulation of the molecular dynamics of nucleic acids. *Curr. Opin. Struct. Biol.* 8:227–236.

Berendsen, H. J. C., J. R. Grigera, and T. P. Straatsma. 1987. The missing term in effective pair potential. *J. Phys. Chem.* 97:6269–6271.

Berger, I., and M. Egli. 1997. The role of backbone oxygen atoms in the organization of nucleic acid tertiary structure: zippers, networks, clamps, and C-H⋯O hydrogen bonds. *Chem. Eur. J.* 3:1400–1404.

Berman, H. M., W. K. Olson, D. L. Beveridge, J. Westbrook, A. Gelbin, T. Demeny, S. H. Hsieh, and A. R. Srinivasan. 1992. The nucleic acid database: a comprehensive relational database of three-dimensional structures of nucleic acids. *Biophys. J.* 63:751–759.

Beveridge, D. L., M. A. Young, and D. Sprous. 1997. Modeling of DNA via molecular dynamics simulation: structure, bending, and conformational transitions. *In* Molecular Modeling of Nucleic Acids. N. B. Leontis and J. SantaLucia, editors. American Chemical Society, Washington, DC. 260–284.

Brion, P., and E. Westhof. 1997. Hierarchy and dynamics of RNA folding. *Annu. Rev. Biophys. Biomol. Struct.* 26:113–137.

Caspar, D. L. D. 1995. Problems in simulating macromolecular movements. *Structure.* 3:327–329.

Cate, J. H., A. R. Gooding, E. Podell, K. H. Zhou, B. L. Golden, C. E. Kundrot, T. R. Cech, and J. A. Doudna. 1996. Crystal structure of a group I ribozyme domain—principles of RNA packing. *Science.* 273:1678–1685.

Cheatham, T. E., J. L. Miller, T. Fox, T. A. Darden, and P. A. Kollman. 1995. Molecular dynamics simulations on solvated biomolecular systems: the particle mesh Ewald method leads to stable trajectories of DNA, RNA and proteins. *J. Am. Chem. Soc.* 117:4193–4194.

Choi, B. S., and A. G. Redfield. 1985. Nuclear magnetic resonance observation of the triple interaction between A9 and AU12 in yeast tRNA^{Phe}. *Nucleic Acids Res.* 13:5249–5254.

Choi, B. S., and A. G. Redfield. 1986. NMR study of isoleucine transfer RNA from *Thermus thermophilus. Biochemistry.* 25:1529–1534.

Choi, B.-S., and A. G. Redfield. 1995. Proton exchange and basepair kinetics of yeast tRNA^{Phe} and tRNA^{Asp}. *J. Biochem.* 117:515–520.

Clarage, J. B., T. Romo, B. K. Andrews, B. M. Pettitt, and G. N. Phillips. 1995. A sampling problem in molecular dynamics simulations of macromolecules. *Proc. Natl. Acad. Sci. USA.* 92:3288–3292.

Correll, C. C., B. Freeborn, P. B. Moore, and T. A. Steitz. 1997. Metals, motifs and recognition in the crystal structure of a 5S rRNA domain. *Cell.* 91:705–712.

Dallas, A., and P. B. Moore. 1998. The loop E-loop D region of *Escherichia coli* 5S rRNA: the solution structure reveals an unusual loop that may be important for binding ribosomal proteins. *Structure.* 5:1639–1653.

Darden, T., D. York, and L. Pedersen. 1993. Particle mesh Ewald: an $N \cdot \log(N)$ method for Ewald sums in large systems. *J. Chem. Phys.* 98:10089–10092.

Derewenda, Z. S., L. Lee, and U. Derewenda. 1995. The occurrence of C-H⋯O hydrogen bonds in proteins. *J. Mol. Biol.* 252:248–262.

Dirheimer, G., G. Keith, P. Dumas, and E. Westhof. 1995. Primary, secondary, and tertiary structures of tRNAs. *In* tRNA: Structure, Biosynthesis, and Function. D. Söll and U. RajBhandary, editors. American Society for Microbiology, Washington, DC. 93–126.

Dock-Bregeon, A. C., B. Chevrier, A. Podjarny, J. Johnson, J. S. de Bear, G. R. Gough, P. T. Gilham, and D. Moras. 1989. Crystallographic structure of an RNA helix: $[U(UA)_6A]_2$. *J. Mol. Biol.* 209:459–474.

Engler, E., and G. Wipff. 1994. MD Draw: A Program of Graphical Representation of Molecular Dynamics Trajectories. Université Louis Pasteur de Strasbourg, France.

Essmann, U., L. Perera, M. L. Berkowitz, T. Darden, H. Lee, and L. G. Pedersen. 1995. A smooth particle mesh Ewald method. *J. Chem. Phys.* 103:8577–8593.

Feig, M., and B. M. Pettitt. 1997. Experiment vs force fields: DNA conformation from molecular dynamics simulations. *J. Chem. Phys. B.* 101:7361–7363.

Friederich, M. W., E. Vacano, and P. J. Hagerman. 1998. Global flexibility of tertiary structure in RNA: yeast tRNA^Phe as a model system. *Proc. Natl. Acad. Sci. USA.* 95:3572–3577.

Gautheret, D., S. H. Damberger, and R. R. Gutell. 1995. Identification of base-triples in RNA using comparative sequence analysis. *J. Mol. Biol.* 248:27–43.

Gautheret, D., and R. R. Gutell. 1997. Inferring the conformation of RNA base pairs and triples from patterns of sequence variation. *Nucleic Acids Res.* 25:1559–1564.

Hall, K. B., J. R. Sampson, O. C. Uhlenbeck, and A. G. Redfield. 1989. Structure of an unmodified tRNA molecule. *Biochemistry.* 28: 5794–5801.

Heerschap, A., C. A. G. Haasnoot, and C. W. Hilbers. 1982. Nuclear magnetic resonance studies on yeast tRNA^Phe. I. Assignment of the iminoproton resonances of the acceptor and D stem by means of NOE experiments at 500 MHz. *Nucleic Acids Res.* 10:6981–7000.

Hermann, T., P. Auffinger, W. G. Scott, and E. Westhof. 1997. Evidence for a hydroxide ion bridging two magnesium ions at the active site of the hammerhead ribozyme. *Nucleic Acids Res.* 25:3421–3427.

Hermann, T., P. Auffinger, and E. Westhof. 1998. Molecular dynamics investigations of the hammerhead ribozyme RNA. *Eur. J. Biophys.* 27:153–165.

Hou, Y. M. 1994. Structural elements that contribute to an unusual tertiary interaction in a transfer RNA. *Biochemistry.* 33:4677–4681.

Hünenberger, P. H., A. E. Mark, and W. F. van Gunsteren. 1995. Fluctuation and cross-correlation analysis of protein motions observed in nanosecond molecular dynamics simulations. *J. Mol. Biol.* 252:492–503.

Hyde, E. I., and B. R. Reid. 1985a. Assignment of the low-field ^1H NMR spectrum of *Escherichia coli* tRNA^Phe using nuclear Overhauser effects. *Biochemistry.* 24:4307–4314.

Hyde, E. I., and B. R. Reid. 1985b. NMR studies of ion binding to *Escherichia coli* tRNA^Phe. *Biochemistry.* 24:4315–4325.

Jack, A., J. E. Ladner, D. Rhodes, R. S. Brown, and A. Klug. 1977. A crystallographic study of metal-binding to yeast phenylalanine transfer RNA. *J. Mol. Biol.* 111:315–328.

Jeffrey, G. A., and W. Saenger. 1991. Hydrogen Bonding in Biological Structures. Springer Verlag, Berlin.

Kholod, N. S., N. V. Pan'kova, S. G. Mayorov, A. I. Krutilina, M. G. Shyapnikov, L. L. Kisselev, and V. N. Ksenzenko. 1997. Transfer RNA^Phe isoacceptors possess non-identical set of identity elements at high and low Mg^{2+} concentration. *FEBS Lett.* 411:123–127.

Kintanar, A., D. Yue, and J. Horowitz. 1994. Effect of nucleoside modifications on the structure and thermal stability of *Escherichia coli* valine tRNA. *Biochimie.* 76:1192–1204.

Kochoyan, M., J. L. Leroy, and M. Gueron. 1990. Process of base pair opening and proton exchange in Z-DNA. *Biochemistry.* 29:4799–4805.

Lee, H., T. Darden, and L. Pedersen. 1995a. Accurate crystal molecular dynamics simulations using particle-mesh Ewald: RNA dinucleotides—ApU and GpC. *Chem. Phys. Lett.* 243:229–235.

Lee, H., T. A. Darden, and L. G. Pedersen. 1995b. Molecular dynamics simulation studies of a high resolution Z-DNA crystal. *J. Chem. Phys.* 102:3830–3834.

Leroy, J. L., N. Bolo, N. Figueroa, P. Plateau, and M. Guéron. 1985. Internal motions of transfer RNA: a study of exchanging protons by magnetic resonance. *J. Biomol. Struct. Dyn.* 2:915–939.

Louise-May, S., P. Auffinger, and E. Westhof. 1996. Calculation of nucleic acid conformation. *Curr. Opin. Struct. Biol.* 6:289–298.

Masquida, B., and E. Westhof. 1998. Crystallographic structures of RNA oligoribonucleotides and ribozymes. *In* Oxford Handbook of Nucleic Acid Structure. S. Neidle, editor. Oxford University Press, London. 533–565.

McCammon, J. A., and S. C. Harvey. 1987. Dynamics of Proteins and Nucleic Acids. Cambridge University Press, New York.

Michel, F., and E. Westhof. 1990. Modelling of the three-dimensional architecture of group I catalytic introns based on comparative sequence analysis. *J. Mol. Biol.* 216:585–610.

Moe, J. G., and I. M. Russu. 1990. Proton exchange and base-pair opening kinetics in 5'-d(CGCGAATTCGCG)-3' and related dodecamers. *Nucleic Acids Res.* 18:821–827.

Moras, D., M. B. Comarmond, J. Fisher, R. Weiss, J. C. Thierry, J. P. Ebel, and R. Giegé. 1980. Crystal structure of yeast tRNA^Asp. *Nature.* 288: 669–673.

Moras, D., A. C. Dock, P. Dumas, E. Westhof, P. Romby, J. P. Ebel, and R. Giegé. 1986. Anticodon-anticodon interactions induces conformational changes on tRNA: yeast tRNA^Asp, a model for tRNA-mRNA recognition. *Proc. Natl. Acad. Sci. USA.* 83:932–936.

Patel, D. J., A. K. Suri, F. Jiang, L. Jiang, P. Fan, R. A. Kumar, and S. Nonin. 1997. Structure, recognition and adaptative binding in RNA aptamer complexes. *J. Mol. Biol.* 272:645–664.

Pearlman, D. A., D. A. Case, J. W. Caldwell, W. S. Ross, T. E. Cheatham, D. M. Ferguson, G. L. Seibel, U. C. Singh, P. K. Weiner, and P. A. Kollman. 1994. AMBER 4.1. University of California, San Francisco, CA.

Pearlman, D. A., and S. H. Kim. 1990. Atomic charges for DNA constituents derived from single-crystal x-ray diffraction data. *J. Mol. Biol.* 211:171–187.

Perret, V., A. Garcia, J. Puglisi, H. Grosjean, J. P. Ebel, C. Florentz, and R. Giegé. 1990. Conformation in solution of yeast tRNA^Asp transcripts deprived of modified nucleotides. *Biochimie.* 72:735–744.

Quigley, G. J., and A. Rich. 1976. Structural domains of transfer RNA molecules. *Science.* 194:796–806.

Ravishanker, G., P. Auffinger, D. R. Langley, B. Jayaram, M. A. Young, and D. L. Beveridge. 1997. Treatment of counterions in computer simulations of DNA. *In* Reviews in Computational Chemistry. K. B. Lipkowitz and D. B. Boyd, editors. VCH Publishers, New York. 317–372.

Reid, S. S., and J. A. Cowan. 1990. Biostructural chemistry of magnesium ion: characterization of the weak binding sites on tRNA^Phe(yeast). Implications for conformational change and activity. *Biochemistry.* 29: 6025–6032.

Saenger, W. 1984. Principles of Nucleic Acid Structure. Springer Verlag, New York.

Schindelin, H., M. Zhang, R. Bald, J. P. Fürste, V. A. Erdman, and U. Heinemann. 1995. Crystal structure of an RNA dodecamer containing the *Escherichia coli* Shine-Dalgarno sequence. *J. Mol. Biol.* 249: 595–603.

Serebrov, V., K. Vassilenko, N. Kholod, H. J. Gross, and L. Kisselev. 1998. Mg^{2+} binding and structural stability of mature and in vitro synthesized unmodified *Escherichia coli* tRNA^Phe. *Nucleic Acids Res.* 26:2723–2728.

Söll, D., and U. L. RajBhandary. 1995. tRNA, Structure, Biosynthesis, and Function. American Society for Microbiology, Washington, DC.

Sprinzl, M., C. Horn, M. Brown, A. Loudovitch, and S. Steinberg. 1998. Compilation of tRNA sequences and sequences of tRNA genes. *Nucleic Acids Res.* 26:148–153.

Stein, A., and D. M. Crothers. 1976a. Conformational changes of transfer RNA. The role of magnesium(II). *Biochemistry.* 15:160–167.

Stein, A., and D. M. Crothers. 1976b. Equilibrium binding of magnesium(II) by *Escherichia coli* tRNA^fMet. *Biochemistry.* 15:157–160.

Steiner, T. 1996. C-H⋯O hydrogen bonding in crystals. *Cryst. Rev.* 6:1–57.

Tapia, O., and I. Velazquez. 1997. Molecular dynamics simulation of DNA with protein's consistent GROMOS force field and the role of counterions' symmetry. *J. Am. Chem. Soc.* 119:5934–5938.

Wahl, C. M., and M. Sundaralingam. 1997. C-H⋯O hydrogen bonding in biology. *Trends Biochem. Sci.* 22:97–102.

Weerasinghe, S., P. E. Smith, V. Mohan, Y.-K. Cheng, and B. M. Pettitt. 1995a. Nanosecond dynamics and structure of a model DNA triplex helix in saltwater solution. *J. Am. Chem. Soc.* 117:2147–2158.

Weerasinghe, S., P. E. Smith, and M. Pettitt. 1995b. Structure and stability of a model pyrimidine-purine-purine DNA triple helix with a GC·T mismatch by simulation. *Biochemistry.* 34:16269–16278.

Westhof, E., P. Dumas, and D. Moras. 1985. Crystallographic refinement of yeast aspartic acid transfer RNA. *J. Mol. Biol.* 184:119–145.

Westhof, E., P. Dumas, and D. Moras. 1988. Restrained refinement of two crystalline forms of yeast aspartic acid and phenylalanine transfer RNA crystals. *Acta Crystallogr. A.* 44:112–123.

Westhof, E., C. Rubin-Carrez, and V. Fritsch. 1995. The use of molecular dynamics simulations for modelling nucleic acids. *In* Computer Modelling in Molecular Biology. J. M. Goodfellow, editor. VCH, New York. 103–131.

Westhof, E., and M. Sundaralingam. 1986. Restrained refinement of the monoclinic form of yeast phenylalanine transfer RNA. Temperature factors and dynamics, coordinated waters, and base-pair propeller twist angles. *Biochemistry.* 25:4868–4878.

Yang, L., and B. M. Pettitt. 1996. B to A transition of DNA on the nanosecond time scale. *J. Phys. Chem.* 100:2564–2566.

York, D. M., W. Yang, H. Lee, T. Darden, and L. G. Pedersen. 1995. Toward the accurate modeling of DNA: the importance of long-range electrostatics. *J. Am. Chem. Soc.* 117:5001–5002.

Young, M. A., and D. L. Beveridge. 1998. Molecular dynamics simulations of an oligonucleotide duplex with adenine tracts phased by a full helix turn. *Biophys. J.* 281:675–687.

Young, M., G. Ravishanker, and D. L. Beveridge. 1997. A 5-nanosecond molecular dynamics trajectory for B-DNA: analysis of structure, motions, and solvation. *Biophys. J.* 73:2313–2336.

Yue, D., A. Kintanar, and J. Horowitz. 1994. Nucleoside modifications stabilize Mg^{2+} binding in *Escherichia coli* tRNA[Val]. An imino proton NMR investigation. *Biochemistry.* 33:8905–8911.

Zichi, D. A. 1995. Molecular dynamics of RNA with the OPLS force field. Aqueous simulation of a hairpin containing a tetranucleotide loop. *J. Am. Chem. Soc.* 117:2957–2969.